This article has been accepted for publication in IEEE/OSA Journal of Lightwave Technology. This is the author's version which has not been fully edited and content may change prior to final publication. Citation information: DOI 10.1109/JLT.2023.3261706

Resonant couplings in U-shaped fibers for biosensing

Carolina Londero, Martina Delgado-Pinar, Christian Cuadrado-Laborde, and Miguel V. Andrés, *Senior Member, IEEE*

***Abstract*—U-shaped tight curvatures in optical fibers lead to resonant couplings between the fundamental and higher order modes that are sensible to different parameters, such as strain or temperature, for example. The optical response of the sensor consists on the shift of the resonant wavelength of the coupling. In the case of singlemode fibers, the coupling involves a so-called "cladding mode" and, due to its evanescent field, the curved region will be sensible to changes in the external medium, as well. In this paper, we present the fabrication and characterization of a robust, easy-to-make, U-shaped fiber sensor based on singlemode telecom fiber and its application for biosensing. The resonant nature of the sensing mechanism presents the advantage of large dynamic ranges for RI variations without the ambiguity of other techniques such as interferometry. We studied the performance of the U-shaped fiber sensor for different bending radii, to optimize its sensitivity and detection limit at 1550 nm operation wavelength, as well as the effect of temperature on its response. The shift of the resonant wavelength was measured in detail as a function of the external RI within the range [1.33-1,37]; the detection limit was established in $(3.71\pm0.03)\times10^{-5}$ RIU. Furthermore, the device was successfully tested as a proof of concept biosensor, using a system model antigen-antibody (BSA-aBSA.)**

***Index Terms*— optical fiber biosensors, U-shaped sensors, biosensing, optical fiber modes, refractometer.**

I. Introduction

THE development of photonic biosensors using optical waveguides and nanostructures is a topic of great interest in the last years, both in industry and academy [1-3]. In particular, optical fibers are well-studied waveguides for a broad range of applications and a number of proposals, based on different mechanisms, are reported in the literature for their use as biosensors [4-6]. The optical fiber can play different roles in the biosensor structure: for example, a tapered fiber can be used to collect the light emitted by a labelled target when biorecognition occurs, or the optical fiber surface can be functionalized to be the sensing platform besides the transducer. Different devices have been proposed for this purpose. Among the evanescent-field-based devices we can find long period gratings (LPGs), tilted fiber Bragg gratings (TFBGs) or BIO-Bragg gratings stamped in tapered fibers [7-10]. Also, surface modes have been exploited for biosensing: optical microfibers can be metallic coated to support surface plasmon resonances [11, 12] and whispering gallery modes in microspheres and microbottles have been demonstrated to show really low detection limits [13,14]. The splice between different types of fibers lead to structures that provide interferometric optical responses sensitive to variations in the external medium, for example single-mode-multimode-single-mode structures [15, 16] or multimode-coreless-multimode structures [17, 18]. Microstructured fibers have been also reported as possible platforms to develop novel biosensors [19].

Here, we propose a device which does not include any additional element different from the pristine optical fiber itself to work as a label-free biosensor; this means that there is not any post-processing of the standard telecom fiber appart from the chemical functionalization. A U-shaped section of fiber and a semi-ellipsoidal section of fiber have been demonstrated to be feasible sensors [20, 21]. In most of the works reported in the literature multimode fibers are used, whether microfibers [22], multimode fibers [23] or decladded fibers [24]. In most of those cases, a description of the propagation of the light in the fiber is based on geometrical rays and the interference between them is the mechanism that explains the results. Interferometry-based methods show the limitation of the periodicity of the fringes, which introduces some ambiguity on the readout of the refractometers or sensors.. In this paper, we rely in a more precise modal description of the propagation of light in the fiber to interpret the findings [25, 26]. In addition, we consider single-mode fibers, which result in more robust devices when compared to microfiber-based devices.

This paper was submitted on 29th, November, 2022. This research was funded by the Ministerio de Ciencia e Innovación/Agencia Estatal de Investigación of Spain (MCIN/AEI/10.13039/501100011033) and co-funded by the European Union "ERDF A way of making Europe", grant number PID2019-104276RB-I00; the Generalitat Valenciana of Spain, grant number PROMETEO/2019/048; and the European Commission, grant number H2020-MSCARISE-2019-872049.

C. M. Londero, was with the Faculty of Exact Sciences, Engineering and Surveying, Rosario, S2000BTP Arg. She is now with the Institute of Physics of Rosario, CONICET UNR, S2000EKF Argentina (e-mail: londero@ifir-conicet.gov.ar).

Martina Delgado-Pinar is with the Laboratory of Fiber Optics, Department of Applied Physics – ICMUV, Universitat de València, 46100 Burjassot, Valencia, SPAIN (e-mail: martina.delgado@uv.es , website: www.uv.es/lfo)

C. A. Cuadrado-Laborde is at the Institute of Physics of Rosario, CONICET UNR, S2000EKF Argentina, and Full Professor at Pontificia Universidad Católica Argentina 'Santa María de los Buenos Aires' (e-mail: christiancuadrado@uca.edu.ar).

Miguel V. Andrés is with the Laboratory of Fiber Optics, Department of Applied Physics – ICMUV, Universitat de València, 46100 Burjassot, Valencia, SPAIN (e-mail: miguel.andres@uv.es , website: www.uv.es/lfo)

This article has been accepted for publication in IEEE/OSA Journal of Lightwave Technology. This is the author's version which has not been fully edited and content may change prior to final publication. Citation information: DOI 10.1109/JLT.2023.3261706

II. OPERATION PRINCIPLE

The bending of a stripped, conventional singlemode fiber induces a perturbation in the refractive index profile of the fiber, due to geometric and strain-optic effects. This perturbation breaks the orthogonality of the modes that propagate in a straight fiber, leading to the coupling of energy from the core mode to cladding modes. The coupling of energy occurs in a resonant manner, that is, a phase-matching condition between the modes involved in the phenomenon must be accomplished. Then, the coupling between the core mode and each cladding mode will take place at those optical wavelengths meeting this condition. At the end of the stripped, curved section, the optical power coupled to the cladding modes will be absorbed by the polymer protecting the silica fiber. As a result, the transmittance of the device will consist on a series of attenuation notches, whose central wavelength will be set by different parameters: the curvature and the refractive indices (RI) of the silica material and the external medium (n_{ext}). A detailed analysis of the modal description of the problem can be found in [25]. Only when many cladding modes are involved, ray models can provide a good description of the effective attenuation produced by the continuous coupling of power from the fundamental mode to the cladding modes. Here, we will work in a range of parameters in which few modes are involved and individual couplings between modes are observed.

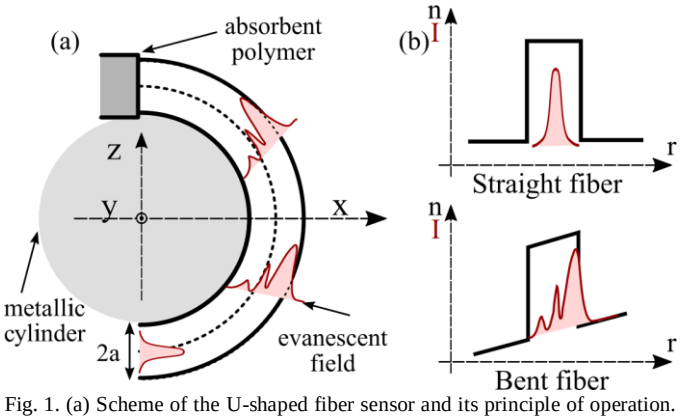

Fig. 1. (a) Scheme of the U-shaped fiber sensor and its principle of operation. (b) Qualitative representation of the optical fields in straight singlemode fiber (core mode) and a bent singlemode fiber (cladding mode) were the black curve represents the refractive index profile of the fiber (n) and the red curve the intensity of the fields (I).

Figure 1 shows a scheme of the operation principle of the device. The resonant behavior of the device constitutes the main difference between our approach and those other U-shaped fibers based refractometers whose operation principle is explained by means of interferometric effects and ray propagation models. It should be noted that using resonant phenomena for determining the external RI overcomes the ambiguity inherent to interferometric methods due to the periodicity of the fringe pattern. Also, when comparing our devices to others reported in the literature, the radii we employ for our U-shaped fibers are bigger ($R \in [5,7]$ mm) [20, 24], as well as the fiber diameters [22], for obtaining resonant wavelengths at the infrared telecom spectral range, which results in a higher robustness of the sensors, and limits losses due to curvature.

III. FABRICATION AND PHYSICAL CHARACTERIZATION

Figure 1 (a) shows a scheme of the U-shaped fiber sensor. SMF-28e standard telecom fiber was used for fabricating the devices. A stripped section of fiber was curved around a metallic cylinder (Fig. 1 (a)). As depicted in Fig. 1 (b), the light coupled to the cladding mode is asymmetrically distributed, mostly next to the interface silica-air. Thus, the loss due to absorption and scattering in the interface silica-metal will be negligible. The length of the stripped section was half the perimeter of the cylinder. The polymer coating was stripped from the fiber using an acetone bath to avoid irregularities on the surface of the fiber. We tested that, using this procedure, the attenuation notches of the resonances were neater. The fiber was attached to the cylinder surface using cyanoacrylate based commercial glue over the polymer coated section. It is worth noting that this doesn't have any effect on light propagation in the fiber. Special attention was paid to apply the same stress to all the fibers during the fabrication process.

Figure 2 (a) shows an example of the transmission spectra measured for two radii of the cylinders: 5.25 and 5.50 mm. Each one shows two resonances for each cylinder, corresponding to two different cladding modes. The spectra were measured using a broadband LED source centered at 1550 nm (spectral range: 200 nm, optical power: 1.7 mW, in-house electronic power supply and controllers) and an OSA (Yokogawa AQ6375, range: 1200-2400 nm, resolution: 20 pm). The free spectral range (FSR) between the notches is larger than 30 nm, as it can be noted in the measurements. In this particular example, for the peak labelled with R_1, the attenuation is higher −18.3 dB (measured from the maximum at both sides), and the 3-dB bandwidth is 17.6 nm. The resonant wavelengths of the attenuation notches could be determined by the OSA using their automatic analysis to do so. We analyzed several spectra (that is, fitting the data ourselves to an attenuation notch) to check that the function of the OSA was operating properly.

For the two spectra shown in the figure, the resonant wavelength, λ_R, shifts towards a longer wavelength for a smaller radius. This feature was measured in detail for the resonance R_1, using cylinders of radius ranging from 5.00 mm to 6.75 mm, with a 0.25 mm step. The small step in radius ensures that we are following the evolution of the same coupling within this range. The results are shown in Fig. 2 (b).

Within the measured range, the results show a decreasing trend of the resonant wavelength as the radius of curvature is increased, for the cylinders surrounded by air (n_{ext} = 1) Moreover, this trend is linear (R^2 = 0.997), with a slope −60.2±1.4 nm/mm. Since the final objective of this work is to test this device as a biosensor, we repeated the measurements for the stripped fiber surrounded by water (n_{ext} = 1.33288). To do so, the device was immersed in a glass beaker containing

This article has been accepted for publication in IEEE/OSA Journal of Lightwave Technology. This is the author's version which has not been fully edited and content may change prior to final publication. Citation information: DOI 10.1109/JLT.2023.3261706

the fluid to test, the complete immersion of the U-shaped loop ensured the fibers outer surface full contact to the surrounding medium. The inset shows the shift of the notch to a longer λ_R when the sensor is immersed in water (resonance R_1). Apart from that overall shift, the trend of the resonant wavelength shift with the radius of curvature remains also linear ($R^2 = 0.995$ and slope -60.4 ± 1.9 nm/mm). Both sets of data show that the spectral position of a same resonance changes equally with the curvature, thus the election of the most convenient radius of the devices (which implies the most convenient resonance) will not be affected by the external medium to be used in the assays.

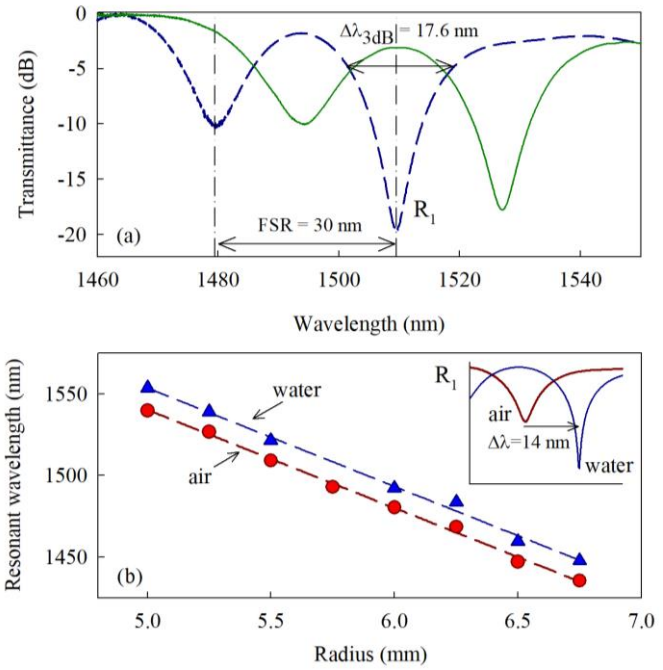

Fig. 2. (a) Transmission spectra of U-shaped devices of radius 5.50 mm (dashed line) and 5.25 mm (continuous line). (b) Resonant wavelength as a function of the radius for external media air (circles) and water (triangles). Inset: transmission spectra of R_1 in air, and immersed in water (n_{ext} = 1.33288).

Stress and temperature change the refractive index of silica and/or the radius of the cylinder and, as a result, the spectral position of the resonance. As said before, special attention was paid to apply the same stress in all devices during the fabrication process. However, the performance of the device will change with temperature, due to thermo-optic effect and also because of dilatation on the metallic cylinder, thus we performed an evaluation of this effect. We traced the changes in the transmission spectrum of a resonance as the temperature was varied from −10ºC to 80ºC (step: 2ºC) in a thermal chamber; the spectra were recorded after the temperature was stabilized for each data point. Figure 3 (a) shows the spectra at both extremal temperatures of this range and at room temperature (19.2 ºC). The first conclusion is that the attenuation does not change significantly in the whole range, neither does the 3-dB bandwidth (20.0, 20.4 and 20.8 nm for the three spectra depicted in Fig. 3 (a), for increasing temperatures). The shape of the resonance neither does change significantly, especially its slope at the middle point of the edge: at $T = -10$ dB, the slopes of the edges are 2.096±0.009, 1.977±0.012 and 1.8881±0.0011 dB/ºC for increasing temperatures, that is, a maximum deviation in the sensitivity below 10% in terms of variation of transmittance. We pay attention to this value (and not only to the wavelength shift) since it determines the sensitivity of the sensor when measuring variations of transmittance to interrogate the device as a refractometer or a biosensor [9, 16].

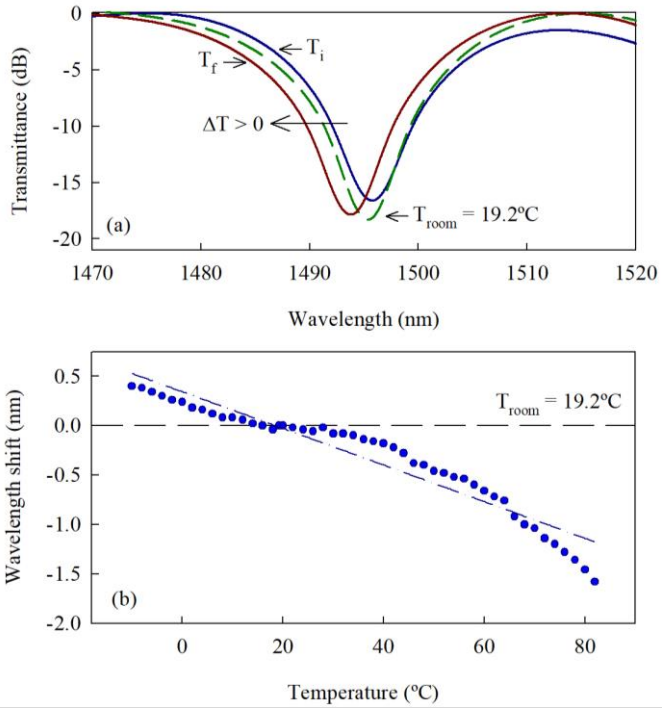

Fig. 3. (a) Transmission spectra of a U-shaped fiber sensor as a function of temperature, for $T_i = -10$ ºC, T_{room} and $T_f = 80$ ºC. (b) Measurement in detail of the wavelength shift of the resonance in the range [−10º, 80º]

Figure 3 (b) shows the data for the evolution of the spectral position of the resonance depicted in Fig. 3 (a) in the [−10ºC, 80ºC] temperature range. A general monotonically decreasing trend is observed. A linear fit is included in the graph as a guideline (average slope: −18.5±0.8 pm/ºC), however it is clear that the data does not fit to a pure linear behavior (R^2=0.917). Two inflection points can be observed (18ºC and 64ºC) separating three temperature ranges. Nevertheless, apart from these two anomalous points, the behavior is pretty linear within each temperature range, even though the slopes are different. We will show later that the time response of our device as a biosensor is about 30 minutes as a maximum, thus a significant change in temperature is not expected during the lapse time used for running a test. It is also worth to note that the total wavelength shift in the wide temperature range [−10, 80] ºC is below 2 nm, which is a tenth part of the 3-dB bandwidth of this resonance (20.4 nm for room temperature, as said). Moreover, if we consider the range of temperatures around the room temperature (±5ºC), where the biomolecules will be active, the wavelength shift with temperature is 6 pm, which is below our resolution, as we will see. We can conclude then that the influence of

temperature on the performance of the device is, at worst, a fine correction to the wavelength shift due to variations in n_{ext}, which will be studied in the next section. We have already shown a first example of this: the inset in Fig. 2 (b) shows the spectra for n_{ext} = 1 and 1.33288, with a wavelength shift between them of 14.5 nm.

Considering all of the above, even though our device is not temperature independent and that this is a parameter that should be taken into account and controlled if possible, we can conclude that the effect of temperature on the performance of the sensor is a secondary contribution to the wavelength shift when compared to the impact of the variation in n_{ext}, mainly because of the short time that the measurements take.

IV. CHARACTERIZATION AS A REFRACTOMETER

The objective of this work is to show a proof of concept of this device as a biosensor. The operation principle in this case is that a change in the external medium will lead to a variation in the spectral position of the resonance, because of the overlapping of the evanescent field with the changes occurring at the external medium. Then, the characterization of the device as a refractometer for variations in n_{ext} will determine parameters such as sensitivity or detection limit of the sensor, in terms of refractive index unit (RIU). The antibodies are usually in aqueous media, thus in this section we will explore the performance of our device as a refractometer for indices similar to that of water.

TABLE I
OPTICAL FEATURES FOR RESONANCES OBSERVED IN DEVICES A AND B

	3-dB bandwidth (nm)	Attenuation (dB)	λ_R (air) (nm)
A		RADIUS: 5.25 MM	
RA_1	15.4	10.5	1494.08
RA_2	17.8	16.1	1527.53
RA_3	23.5	11.7	1607.18
B		RADIUS: 6 MM	
RB_1	22.5	19.3	1506.97
RB_2	26.8	14.8	1535.29
RB_3	17.0	10.7	1593.32

We tested devices of two radii: 5.25 mm (device A) and 6 mm (device B) and monitored the redshift for their resonant wavelengths. The optical features of the resonances observed for these two devices are compiled in Table I. It is worth to note that the FSR is larger than 33 nm for device A, and 28 nm for device B, both larger than the corresponding 3-dB bandwidth of the notches. The attenuation of the notches (measured in air) exceeded 10 dB in all cases. Since the couplings correspond to different cladding modes and, consequently, different dispersion curves of their modal indices, we wanted to explore how the sensitivity of the sensor changes for different geometries and resonances.

The measurement in detail of the wavelength shift of RA_1, RA_2, RB_1, RB_2 and RB_3 as n_{ext} varies is shown in Fig. 5 (RA_3 is not shown because it shifted further than the range of our LED source). The wavelength shift is positive as n_{ext} increases, and the data follow a linear trend, although smooth inflexion points can be observed in some cases, but they are not as significant as in the case of the temperature. The slopes of these linear fits are the sensitivity of the sensor in terms of RIU of n_{ext}, for each device and resonance. To perform this measurement, we immersed the devices in a solution of EtOH in H_2O, and the n_{ext} was varied by adding EtOH to the mixture.

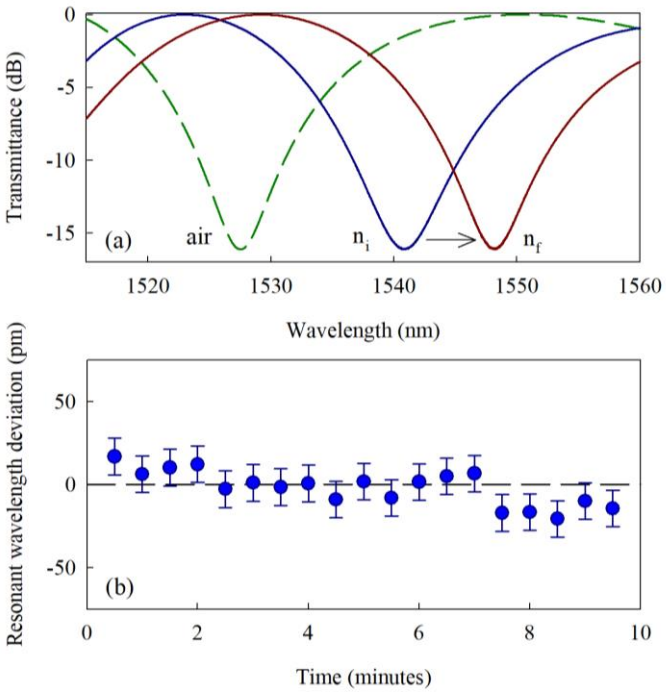

Fig. 4. (a) Transmission spectra of RA_2 when the external medium is air (dashed line), and EtOH-H_20 solutions of refractive indices n_i=1.333 and n_f=1.361. (b) Measurement of the uncertainty on the determination of the resonant wavelength, 11 pm.

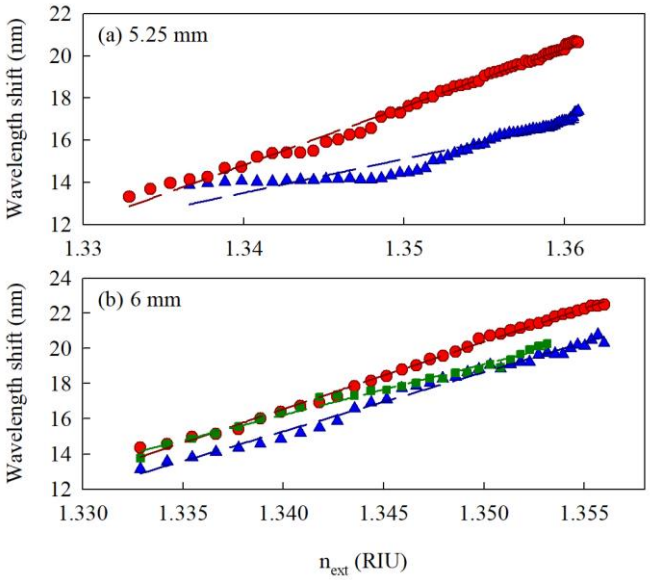

Fig. 5. Wavelength shift of the resonant wavelength for two devices: (a) radius 5.25 mm, resonance RA_1 (triangles) and RA_2 (circles); (b) radius 6 mm, resonance RB_1 (triangles), RB_2 (circles) and RB_3 (squares). Linear fits are included for each set of data.

The solution was agitated during the measurements to ensure a rapid and homogeneous dilution. To calculate n_{ext} as a function of the mole fraction of EtOH present in the solution, x, at 25 ºC and 632.8 nm, a fit to the data of Fig. 17 in reference [27] was used: $n_{ext}(x) = 1.33288 + 0.179258\,x - 0.380008\,x^2 + 0.351867\,x^3 - 0.124503\,x^4$ (please note there are two typos at the equation provided in the reference). We estimated the resolution of our measurements by measuring repeatedly the resonant wavelength of a resonance in air over a lapse time of 10 minutes; we concluded that the resolution of our measurements is a wavelength shift of 11 pm, see Fig. 4(b): the error bars are the standard deviation of the collected data; each spectrum was analyzed to extract its minimum using a peak fit. This resolution takes into account the resolution of the equipment, the bandwidth of the notches, and other sources of noise in the measurement, including the possible variations of temperature that could take place in standard research laboratory conditions [28]. In particular, in our experiment, having in mind the 3-dB bandwidths and attenuation levels, an accurate determination of the minimum of the resonance is crucial. These 11 pm corresponds to a 0.05 % part of the typical 3-dB bandwidth that we measured for most resonances. With this data, the calculated sensitivities and detection limits are presented in Table II.

TABLE II
SENSITIVITY AND DETECTION LIMITS IN TERMS OF n_{ext} RIU

	Sensitivity (nm/RIU)	Detection limit (RIU)	R^2 of the linear fit
RA_1	164±6	$(6.7\pm0.2)\times10^{-5}$	0.923
RA_2	276±3	$(3.99\pm0.04)\times10^{-5}$	0.992
RB_1	339±6	$(3.24\pm0.06)\times10^{-5}$	0.994
RB_2	382±4	$(2.88\pm0.03)\times10^{-5}$	0.998
RB_3	288±7	$(3.82\pm0.09)\times10^{-5}$	0.993

From this data obtained for these two specific devices of given radius and considering the characterized couplings we observe that, contrarily to expected, a tighter curvature does not necessarily lead to a better sensitivity and detection limit (even though the evanescent field is expected to be larger at higher curvatures). The results indicate that, for the best cases, the sensor of 6 mm in radius shows a sensitivity 1.4 times higher than that of 5.25 mm. Also, the difference in sensitivities between two adjacent resonances of the same device differs in 12%. Thus, the proper selection of the radius and the resonance will improve the performance of our biosensor: we used RB_2 for our biosensing tests.

We carried out an additional experiment to explore the possibility of using the same device for several tests. Figure 6 shows a series of chained tests, where we monitored the resonant wavelength for RA2 and RB1 over time. The U-shaped sensor was immersed in and out of different H2O-EtOH dilutions (0, 20, 40 y 60 % v/v, that is n_{ext} = 1.333, 1.344, 1.354, 1.362). The sensor was immersed in the solution, and after it was retrieved, it was dried using nitrogen gas to evaporate any possible leftover on the surface, to ensure that there was not any liquid film covering it. All the process, including the drying process is shown in the graph, the data of the spectral position of R was registered every 30 s. It is observed that every time the resonant wavelength is measured in air the notch returns to its original position, with a maximum deviation of 1 nm in a total wavelength shift of 22 nm in worst cases, see Fig. 5 (b). It is also worth to note than the wavelength shifts obtained for the different dilutions of EtOH-H_2O fit with the sensitivity previously measured in Fig. 5, even when these were different experiments carried out in different days. As a conclusion from its refractometric characterization, a single device could be used repeatedly for several tests. Thus, it would be expected that a convenient anchoring of the BSA proteins to the fiber surface and a proper cleaning method of the antibodies aBSA would allow recycling the device to be used multiple times for biosensing while maintaining its performance in terms of sensitivity and detection limits.

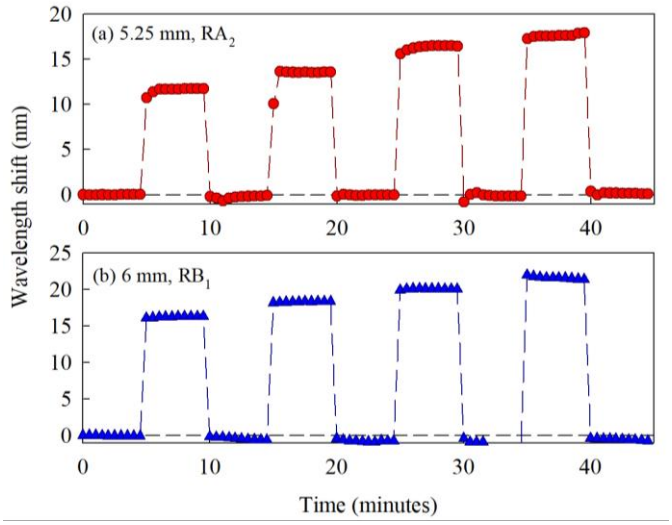

Fig. 6. Measurement of chained measurement of the wavelength shift of two devices for different values of n_{ext} (1.333, 1.344, 1.354, 1.362, from left to right)

V. PROOF OF CONCEPT FOR BIOSENSING

We chose a Bovin Serum Albumin (BSA)/antiBSA rabbit IgG (aBSA) antigen/antibody system since this is a well stablished model for biosensing proofs of concept. The chemicals are commercial products from Sigma-Aldrich (Madrid, Spain). We attached the antigens, BSA proteins to the fiber surface, and they biorecognized the antibodies aBSA present in a buffered solution, binding each other. This led to a refractive index variation in the vicinities of the fiber surface, over the region where the evanescent field of the cladding modes extend. For our case, we estimated the depth of the BSA/aBSA film in 10 nm, attending to the simulations and experiments carried out in previous works [10].

The functionalization of the fibers' surface was done before the fabrication of the U-shaped sensor. First, the fibers were rinsed in DI water and air dried. Second, they were immersed in a solution of 50 $\mu g \cdot mL^{-1}$ of BSA proteins in a buffered PBS solution in miliQ water, where they stayed for 120 minutes at constant temperature (37ºC). The BSA proteins anchored to

This article has been accepted for publication in IEEE/OSA Journal of Lightwave Technology. This is the author's version which has not been fully edited and content may change prior to final publication. Citation information: DOI 10.1109/JLT.2023.3261706

the fiber surface due to ionic bonds between them and the -OH groups. After this lapse time, the fibers were DI water rinsed, air dried and stored at 4ºC until use. They were later retieved, and once at room temperature the U-shaped sensors were fabricated according to the procedure described in section III, with a radius curvature of 6 mm. We used a resonance centered at 1539 nm in air, that is, corresponding to a resonance RB_2.

Figure 7 (a) shows the spectra of the device before and after the incubation of aBSA antibodies; both spectra were recorded when the U-shaped bare section of the fiber was immersed in a drop of PBS solution in miliQ water containing 50 $\mu g \cdot mL^{-1}$ of aBSA antibodies. The dashed curve corresponds to the spectrum just at the beginning of the incubation, that is, when the recognition BSA/aBSA has not occurred yet, thus we can consider this spectral position of the resonance as the origin of wavelength shift. The continuous line shows the spectrum at the maximum wavelength shift, measured after 27 minutes. Both notches are well resolved, the shift is roughly a tenth part of the 3-dB bandwidth (11.84 nm), and 130 times our resolution.

We monitored the resonant wavelength with time (step: 30 s) as the biorecognition took place, see Fig. 7 (b). The maximum wavelength shift was reached after 27 minutes, with a value of 1.43±0.02 nm. After that, a slight blue shift (27 pm) was detected, due to de-adsorption of aBSA molecules: at this point, we stopped the assay. After 15 minutes, 90% of the final wavelength shift was reached, thus we can consider that this is the time response of our biosensor. This is a parameter to be taken into account to disregard the temperature variations that could occur during this lapse time when this experiment is performed without any temperature stabilization.

Here we intend to show a proof of concept of our biosensor, and further characterization in terms of biochemical parameters is out of the scope of this work. Thus, we did not proceed with a complete immunoassay study, testing different concentrations of the aBSA targets. Nevertheless, in order to estimate the sensitivity and detection limit of our biosensor in terms of concentration of aBSA, we will assume that 50 $\mu g \cdot mL^{-1}$ is still in the linear range of the biosensor, which is a conservative assumption. From this data, the estimated sensitivity would be (28.6±0.4) pm/($\mu g \cdot mL^{-1}$). It is worth noting that some techniques have been proposed to improve this parameter by including additional layers of high refractive index as in [29]. Since we determined previously that the resolution of our system is 11 pm, we estimate the detection limit to be (385±5) $ng \cdot mL^{-1}$. These results are in the same order of magnitude of previous works we have performed with the same BSA/aBSA system, but a different photonic biosensor based on a different operation principle [10]. As said before, the calculation of sensitivity and detection limit presented here arises from a conservative assumption. From previous works [10, 30] we know that the linear range of BSA/aBSA biosensor ends around 10 $\mu g \cdot mL^{-1}$, but since those transducers rely on different operation principle (diffractive grating), we chose a aBSA concentration that was further indeed of that limit, to be sure that we were observing the maximum possible response of the biosensor.

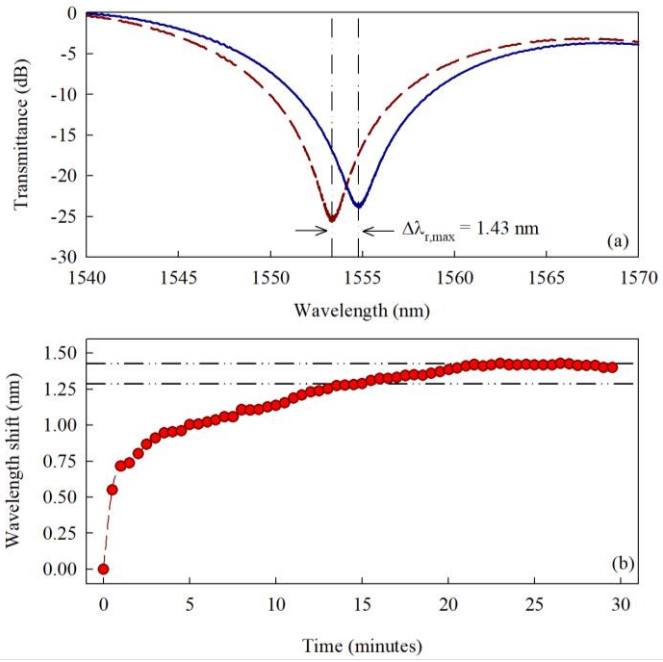

Fig. 7. Proof of concept of the U-shaped biosensor using a BSA/aBSA model. (a) Transmission spectra before (dashed line) and after (continuous line) the incubation of the antibody. (b) Temporal evolution of the wavelength shift, Horizontal lines indicate the maximum and the 90% wavelength shift.

Thus we can expect that a more detailed study would provide detection limits at least a factor of 5 better than this estimate. The biochemical characterization in detail of this biosensor, as well as the study of its capability to be recycled, is work for further research.

VI. CONCLUSIONS

In this work we presented a U-shaped fiber sensor fabricated from conventional, singlemode fiber that only uses a short, bare section of fiber curved with moderated radii. We analyze its principle of operation using a description in terms of resonant coupling between the modes guided by the fibers, in opposition to most of the works in the literature that analyze such devices from an interferometric point of view and ray propagation in multimode fibers. In fact, the resonant nature of our biosensor allows monitoring the wavelength shift of the resonant couplings in a broad RI range without the ambiguity inherent to interferometric procedures. In our case, the minimum FSR between adjacent resonances is larger than 30 nm. This feature, together with the easy manufacture of the devices and their robustness, are great advantages of our approach when compared to other U-shaped fiber sensors.

The sensitivity obtained for the 6 mm radius device is (382±4) nm/RIU and thus comparable or better than results gathered in [16, 17] for wavelength shift based sensors in the same RI range. The detection limit for this resonance is $(2.88\pm0.03)\times10^{-5}$ RIU.

A proof of concept of this device as a biosensor has been presented using a BSA/aBSA antigen/antibody system. This

test shows that the device is capable to detect the recognition of the target in a lapse time of 15 minutes. Our estimation of the sensitivity and detection limit is (28.6±0.4) pm/(μg·mL^{-1}) and (385±5) ng·mL^{-1}, respectively; nevertheless, the perspectives indicate that the reported detection limit is a conservative estimation and that further tests might improve these numbers.

ACKNOWLEDGMENTS

We would like to thank to MSc. Augusto Juste-Dolz and Dr. Estefanía Delgado-Pinar for assistance with doubts in the process of functionalization of the fibers.

REFERENCES

[1] T. Guo, G. Xiao, L. Rovati and Z. He, "Guest Editorial - Guided Lightwaves for Sensors & Measurement Systems: Advanced Techniques and Applications," in *J. of Lightwave Technol.*, vol. 39, no. 12, pp. 3623-3625, June 2021, 10.1109/JLT.2021.3083429.

[2] H. Altug, SH. Oh, S.A. Maier, J. Homola, "Advances and applications of nanophotonic biosensors", *Nat. Nanotechnol.* Vol. 17, no. 5, art. 16 Jan. 2022, 10.1038/s41565-021-01045-5.

[3] C. Dhote, A. Singh and S. Kumar, "*Silicon Photonics Sensors for Biophotonic Applications—A Review*," *IEEE Sensors Journal*, vol. 22, no. 19, pp. 18228-18239, Oct 2022, 10.1109/JSEN.2022.3199663.

[4] M. S. Soares, N. F. Miguel Vidal, Santos, F. M. Costa, C. Marques, S. O. Pereira, C. Leitão, "Immunosensing based on optical fiber technology: Recent Advances," *Biosensors*, vol. 11, no. 9, art. 305, August 2021, 10.3390/bios11090305.

[5] W. Liu, Z. Liu, Y. Zhang, S. Li, Y. Zhang, X. Yang, J. Zhang, L. Yuan, "Specialty optical fibers and 2D materials for sensitivity enhancement of fiber optic SPR sensors: a review," *Optics & Laser Technol.*, vol. 152, art 108167, August 2022, 10.1016/j.optlastec.2022.108167

[6] F. Chiavaioli, Francesco, F. Baldini, S. Tombelli, C. Trono, A. Giannetti, "Biosensing with optical fiber gratings," *Nanophotonics*, vol. 6, no. 4, pp. 663-679, June 2017, 10.1515/nanoph-2016-0178

[7] O. A. Stepustchenko, O. G. Morozov, I. R. Sadykov, G. A. Morozov, P. E. Denisenko, A. N Gorshunova, "Optical refractometric FBG biosensors: problems of development and decision courses," *Proc. SPIE 7992, Optical Technologies for Telecommunications*, 79920D, April 2011, 10.1117/12.887282.

[8] X. Chen, C. Liu, M. D. Hughes, D. A. Nagel, A. V. Hine, L. Zhang, "EDC-mediated oligonucleotide immobilization on a long period grating optical biosensor," *J. of Biosensors & Bioelectron.*, vol. 6, no. 2, 1000173, 2015, 10.4172/2155-6210.1000173.

[9] M. Delgado-Pinar, Q. Shi, L. Poveda-Wong, E. Delgado-Pinar, B. Xu, J. Zhao, J. L. Cruz, M. V. Andrés, "Oligonucleotide-Hybridization Fiber-Optic Biosensor Using a Narrow Bandwidth Long Period Grating," *IEEE Sensors Journal*, vol. 17, no. 17, pp. 5503–5509, 2017, 10.1109/JSEN.2017.2723759.

[10] A. Juste-Dolz, M. Delgado-Pinar, M. Avella-Oliver, E. Fernández, D. Pastor, M. V. Andrés, Á. Maquieira, "BIO Bragg gratings on microfibers for label-free biosensing," *Biosensors & Bioelectronics*, vol. 176, no. 15 art. 112916, March 2021, 10.1016/j.bios.2020.112916.

[11] Y. Wei, J. Hu, P. Wu, Y. Su, C. Liu, S. Wang, X. Nie, L. Liu, "Optical Fiber Cladding SPR Sensor Based on Core-Shift Welding Technology," *Sensors*, vol. 19, no. 5, art. 1202, March 2019, 10.3390/s19051202.

[12] L. Singh, R. Singh, B. Zhang, S. Cheng, B. Kumar-Kaushik, S. Kumar, "LSPR based uric acid sensor using graphene oxide and gold nanoparticles functionalized tapered fiber," *Optical Fiber Technol.*, vol. 53, art. 102043, Dec. 2019, 10.1016/j.yofte.2019.102043.

[13] S. Zhang, H. Wang, J. Xiong, C. Wan, Y. Lu, L. Ang, P. Lv, "A High-Q, Hollow-Core Micro-Bottle Cavity Biosensor for DNA Detection With Low Detection Limit," *J. of Lightwave Technol.*, vol. 40, no. 15, pp. 5345-5351, Aug 2022, 10.1109/JLT.2022.3173409.

[14] S. Subramanian, S. Vincent, F. Vollmer, "Effective linewidth shifts in single-molecule detection using optical whispering gallery modes," *Appl. Phys. Lett.*, vol. 117, no. 15, art. 151106, Oct. 2020, 10.1063/5.0028113.

[15] A. B. Socorro, E. Santamaría, J. Fernández-Irigoyen, I. del Villar, J. M. Corres, F. J. Arregui, I. R. Matías, "Fiber-Optic Immunosensor Based on an Etched SMS Structure," *IEEE J. of Select. Topics in Quantum Electron.*, vol. 23, no. 2, pp. 314-321, March-April 2017, 10.1109/JSTQE.2016.2633819.

[16] P. Ji, S. Jiang, S-S. Lee, "Fiber Reshaping-Based Refractive Index Sensor Interrogated through Both Intensity and Wavelength Detection," Sensors, vol. 19, no. 11, art. 2477, May 2019, 10.3390/s19112477.

[17] N. San Fabián, A. B. Socorro-Leránoz, I. del Villar, S. Díaz, I. R. Matías, "Multimode – Coreless – Multimode Fiber-based Sensors: Theoretical and Experimental Study," *J. of Lightwave Technol.*, vol. 37, no. 15, pp. 3844-3850, 2019, 10.1109/JLT.2019.2921609.

[18] A. Vicente, D. Santano, P. Zubiate, A. Urrutia, I. del Villar, C. Ruiz Zamarreño, "Lossy mode resonance sensors based on nanocoated multimode-coreless-multimode fibre," *Sensors and Actuators B: Chemical*, vol. 304, art. 126955, Oct. 2020, 10.1016/j.snb.2019.126955.

[19] S. A. Pidenko, N. A. Burmistrova, A. A. Shuvalova, A. A. Chibrovaa, Y. S. Skibina, I. Y.Goryacheva, "Microstructured optical fiber-based luminescent biosensing: is there any light at the end of the tunnel? - A review," *Analitica Chimica Acta*, vol. 17, pp. 14-24, Aug. 2018, 10.1016/j.aca.2017.12.010.

[20] K.-C. Chen, Y-L. Li, C-W. Wu, C-C. Chiang, "Glucose Sensor Using U-Shaped Optical Fiber Probe with Gold Nanoparticles and Glucose Oxidase," *Sensors*, vol. 18, no. 4, art. 1217, April 2018, 10.3390/s18041217.

[21] A. N. Castro-Martínez, M. Komanec, T. Nemecek, S. Zvanovec, S. Khotiaintsev, "Fiber optic refractometric sensors using a semi-ellipsoidal sensing element," *App. Opt.*, vol. 55, no. 10, pp. 2574–2579, March 2016, 10.1364/AO.55.002574.

[22] H. Yan, C. Zhang, X. Zhao, Z. Zhen, Q. Li, J. Cao, "Experimental study of liquid refractive index sensing based on a U-shaped micro-fiber," *Optik International J. for Light and Electron Optics*, vol. 126, no. 11-12, pp. 1254-1257, Feb. 2015, 10.1016/j.ijleo.2015.02.051 .

[23] Y. Zhang, M. Lei, H. Hu, Y. Zhao, J. Li, H. Gao, "Determination of refractive index by a U-shaped multimode fiber sensor," Instrumentation Science & Technol., vol. 46, no. 5, pp. 490-501, Jan. 2018, 10.1080/10739149.2017.1419253

[24] A. J. Y. Tan, S. M. Ng, P. R. Stoddart, H. S. Chua, "Theoretical Model and Design Considerations of U-shaped Fiber Optic Sensors: A Review," *IEEE Sensors Journal*, vol. 20, no. 24, pp. 14578-14589, Dec. 2020, 10.1109/jsen.2020.3011173.

[25] M. Reyes, D. Monzón-Hernández, A. Martínez-Ríos, E. Silvestre, A. Díez, J. L. Cruz, M. V. Andrés, "A refractive index sensor based on the resonant coupling to cladding modes in a fiber loop," *Sensors*, vol. 13, no. 9, pp. 11260–11270, Aug. 2013, 10.3390/s130911260.

[26] M. Reyes, "Análisis modal de fibras ópticas curvadas: aplicaciones de sensor,", PhD Dissertation, Dept. Appl. Phys. and Electromagnetism, Universitat de València, May 2017, Spain https://www.educacion.gob.es/teseo/mostrarRef.do?ref=1403019.

[27] A. A. Ghoreyshi, F. A. Farhadpour, M. Soltanieh, A. Bansal, "Transport of small polar molecules across nonporous polymeric membranes: I. Experimental procedures and data analysis," *J. of Membrane Science*, vol. 211, no. 2, pp. 193–214, Jan. 2003, 10.1016/S0376-7388(02)00312-5.

[28] I. M. White, X. Fan, "On the performance quantification of resonant refractive index sensors," *Opt. Express*, vol. 16, no. 2, pp. 1020–1028, Jan. 2008, 10.1364/OE.16.001020.

[29] .S. Bandyopadhyay, I. Del Villar, N. Basumallick, P. Biswas, T. K. Dey, S. Bandyopadhyay, "Long Period Fiber Grating for Biosensing: An Improved Design Methodology to Enhance Add-Layer Sensitivity," *J. Lightwave Technol.*, vol. 36, no. 4, pp. 1178-1184, Feb. 2018, 10.1109/JLT.2017.2754549.

[30] A. Juste-Dolz, M. Delgado-Pinar, M. Avellá-Oliver, E. Fernández, J. L. Cruz, M. V. Andrés, and Á. Maquieira, "Denaturing for nanostructuring: local and periodic UV-laser photodeactivation of protein biolayers to creatre functional patterns for biosensing," *ACS App. Mat. & Interfaces*, vol. 14, pp. 41640−41648, Sept. 2022, 10.1021/acsami.2c12808

This article has been accepted for publication in IEEE/OSA Journal of Lightwave Technology. This is the author's version which has not been fully edited and content may change prior to final publication. Citation information: DOI 10.1109/JLT.2023.3261706

Carolina María Londero was born in Rosario (Argentina) in 1992 and obtained her Physics degree in the Faculty of Exact Sciences, Engineering and Surveying, Rosario, S2000BTP Arg. She is currently a member of the Optics and Photonics Group of the Physics Institute of Rosario (CONICET-UNR) developing her Ph.D thesis entitled "Research and development of optical sensors based on state-of-the-art techniques for the detection of analytes in biological fluids. Applications in Biomedical Physics" as a doctoral fellow from CONICET. During her formation, she participated in two research stays at the Fiber Optic Laboratory, of the University of Valencia, Spain (2018-2019 & 2021). She is a Teaching Assistant at Faculty of Biochemical and Pharmaceutical Sciences (FCByF) as well as at the Faculty of Exact Sciences, Engineering and Surveying (FCEIA) of the National University of Rosario. She has 4 international publications and more than 10 presentations at scientific conferences and meetings.

Martina Delgado-Pinar was born in Valencia (Spain) and, at present, she is Lecturer in Applied Physics at the Department of Applied Physics and Electromagnetism, member of the Laboratory of Fiber Optics research group and the Institute for Science Materials (ICMUV) of the Universitat de València. He received the B.Sc. and Ph.D. degrees in physics from the University of Valencia, Spain, in 2002 and 2008, respectively.

Since 2002, when she graduated, she successively worked as a predoctoral researcher at the Universitat de València, Valencia, Spain and a postdoctoral researcher at the Centre for Photonics and Photonics Materials at the University of Bath, UK (2008-2012). She rejoined the Laboratory of Fiber Optics at 2013 funded by a Juan de la Cierva grant funded by the Ministerio de Ciencia of Spain (2013-2016) and, since then, she worked as an assistant researcher at this group. In 2020 she joined the Department of Electromagnetism of the Universitat de Barcelona as a Lecturer in Electromagnetism, After a brief period, she joined back in 2020 to the Universitat the València as a Lecturer in Applied Physics, her actual position. Her interests include biosensors, in fiber acousto-optics and optomechanics, optical microrresonators, Whispering Gallery Modes and nonlinear optics.

Dr. Delgado-Pinar holds a number of collaborations with other research institutions, including the IFAC-CNR in Florence and the LAFTLA-UCR in Costa Rica, among others. She has been invited visitant researcher in China, Florence, Brazil and Costa Rica. She is member of Optica, EOS and SEDOPTICA. Currently, she serves as the advisor of the student chapter of Optica Photonets-UV at the Universitat de València, and she is the vice-chair of the Women in Optics and Photonics Committee of SEDOPTICA.

Christian Cuadrado-Laborde received his Ph.D. degree in physics from the Universidad Nacional de La Plata (UNLP, Argentina, 2005) and his MEng degree in Electricity and Electronics from the Universidad Nacional de San Luis (UNSL, Argentina, 1999). Since 2005, he has successively served as Postdoctoral Researcher, Assistant Researcher, Associate Researcher, and currently Independent Researcher for the Consejo Nacional de Investigaciones Científicas y Técnicas (CONICET, Argentina, 2005), with workplace in the Instituto de Física Rosario (IFIR, Argentina). He was awarded by the Spanish Ministry of Science with a research fellow position to join the Laboratory of Fiber Optics group of the Universidad de Valencia (UV, Spain) during 2008–2009, since then he has continued working with this group as a visiting Professor. His current research interests include all-fiber lasers and photonic signal processing.

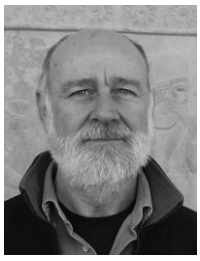

Miguel V. Andrés (SM'2020) was born in Valencia (Spain) in 1957 and, at present, he is Professor at the Department of Applied Physics of the University of Valencia, Spain, being responsible for the leadership and management of the Laboratory of Fiber Optics. He is member of the Institute for Science Materials (ICMUV) of the Universitat de València. He received the B.Sc. and Ph.D. degrees in physics from the University of Valencia, Spain, in 1979 and 1985, respectively.

Since 1983, he has successively served as Assistant Professor, Lecturer, and Professor in the Department of Applied Physics, University of Valencia, Valencia, Spain. After a postdoctoral stay (1984-1987) at the Department of Physics, University of Surrey, U.K., he founded the Laboratory of Fiber Optics at the University of Valencia. His current research interests include photonic crystal fibers, in-fiber acousto-optics and optomechanics, fiber lasers and new fiber-based light sources, fiber sensors, optical microcavities, microwave photonics, and waveguide theory.

Prof. Andrés research activity includes an increasing number of collaborations with Latin America universities and research institutes of Mexico, Argentina and Brazil among others. He is member of Optica, EOS and SEDOPTICA.Spain, in 2002 and 2008, respectively.